applied optics

Sharp bend in two-dimensional optical waveguide based on gradient refractive index structure

Yinghui Cao,[1,2] Raj Mittra,[2,3] Zhenyu Liu,[4] and Jie Zheng[5,*]

[1]College of Computer Science and Technology, Jilin University, 2699 Qianjin Street, Changchun, Jilin 130021, China
[2]EMC Lab, University of Central Florida, Orlando, Florida 32816, USA
[3]King Abdulaziz University, Jeddah 22254, Saudi Arabia
[4]Changchun Institute of Optics, Fine Mechanics and Physics, 3888 East Nanhu Road, Changchun, Jilin 130033, China
[5]College of Electronic Science and Engineering, Jilin University, 2699 Qianjin Street, Changchun, Jilin 130021, China
*Corresponding author: zhengjie@jlu.edu.cn

Received 10 February 2017; revised 29 May 2017; accepted 29 May 2017; posted 30 May 2017 (Doc. ID 286511); published 22 June 2017

In this work, we propose the design of a sharp bend in a two-dimensional optical waveguide which has super-ellipse curve boundaries and a gradient refractive index structure in its core. Numerical simulations are presented to show the efficient light propagation in the waveguide bend, as well as the efficient light coupling between the proposed waveguide bend and a straight waveguide, for TE0 and TM0 modes. The proposed design strategy is also useful for designing other compact optical and photonic components.

OCIS codes: (230.7370) Waveguides; (130.1750) Components.

https://doi.org/10.1364/AO.56.005336

1. INTRODUCTION

Optical waveguide bends are frequently used to connect different optical components in photonic integrated circuits (PICs). Compact optical waveguide bends, which have small bending radius, are useful as potential components for developing high-density PIC devices [1]. However, previous studies have shown that the bending loss of a waveguide bend increases significantly as the bending radius is decreased [1–4]. This in turn may degrade the performance of dense PIC devices. A promising solution is to use sharp bends in silicon-on-insulator (SOI) strip waveguides, which confines propagating light to its core and has very low bending loss [5]. However, it is inefficient to directly couple the SOI waveguide bends with conventional silica-based optical waveguides [6,7]. More recently, sharp waveguide bends based on anisotropic and isotropic metamaterials have been proposed [8–10]. Although metamaterial-based optical waveguide bends have compact size and nearly perfect light transmission, anisotropic and isotropic metamaterials are difficult to fabricate in the optical range. In recent years, a sharp optical waveguide bend based on free-form metamaterial [11] has been reported. By spatially engineering the refractive index of the SOI substrate, free-form metamaterial can be fabricated into difference kinds of nanophotonic components. However, the free-form metamaterial-based components require inverse designing and nanofabrication with resolution of 100 nm, and thus are complicated to implement. In this work, we numerically investigate the possibility of designing a compact optical waveguide bend composed of conventional optical materials, capable of coupling efficiently with conventional silica-based optical waveguides. We present the design of a sharp bend in a two-dimensional optical waveguide, with super-ellipse boundaries and gradient refractive index (GRIN) structure in its core.

2. DESIGN OF THE OPTICAL WAVEGUIDE BEND

To simplify the problem, we use two-dimensional waveguides in this work. Instead of the commonly used circular bend configuration, in our design we choose super-ellipse curves as the shape of boundaries and axis of the waveguide bend, as shown in Fig. 1(a). The axis of the waveguide bend is indicated by the dashed line in Fig. 1(a). The super-ellipse curve can be described by the parametric equations

$$\begin{cases} x = r_s(\cos\theta_s)^{2/n_s} \\ y = r_s(\sin\theta_s)^{2/n_s} \end{cases}, \tag{1}$$

where r_s and θ_s are coordinates of the super-ellipse polar coordinate system. The values of r_s and n_s for the inner boundary, axis, and outer boundary of the waveguide bend are listed in Table 1. The waveguide bend is connected to an input and output waveguide, both of which are straight waveguides with a core width of 1 μm and refractive index of $n_{co} = 1.5$ in its core. The outside medium surrounding the waveguide core is air. Both input and output waveguides support TE0, TE1, TM0, and TM1 modes [12]. The curvature of a parametric curve can be calculated using the equation [13]

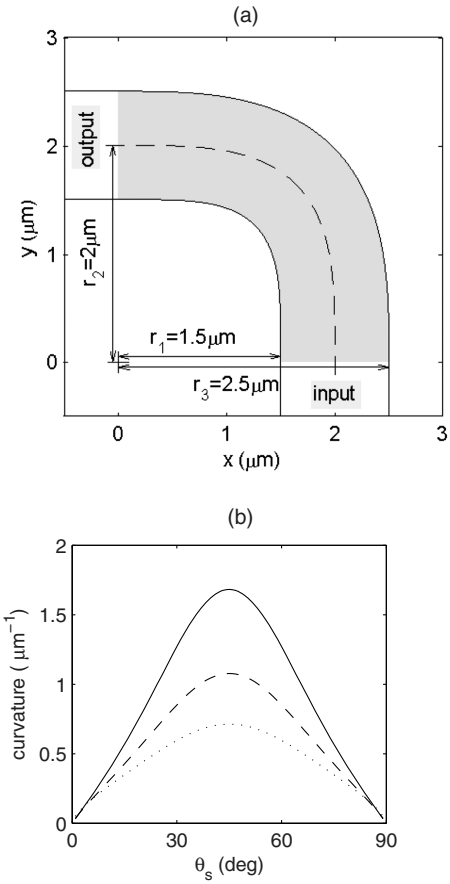

Fig. 1. (a) Structure of the super-ellipse waveguide bend. (b) Curvature along the inner boundary, axis, and outer boundary of the waveguide bend, indicated by solid, dashed, and dotted lines, respectively.

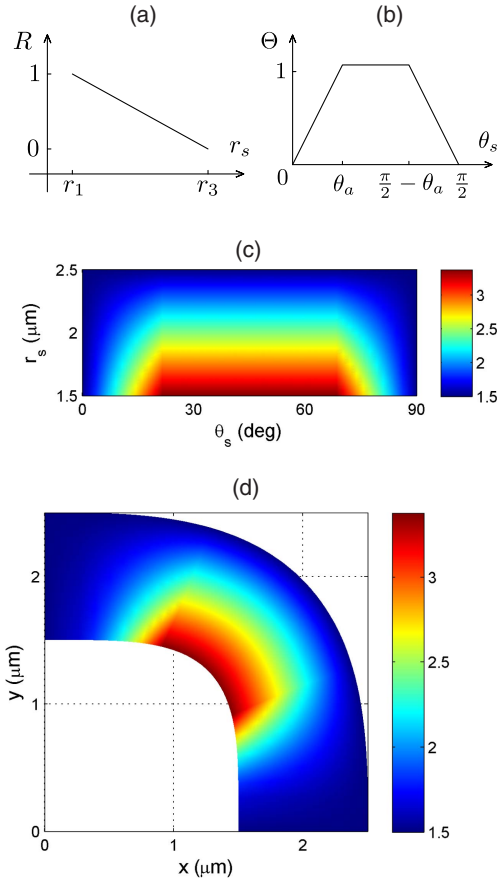

Fig. 2. (a) Curve of $R(r_s)$. (b) Curve of $\Theta(\theta_s)$. (c) Refractive index distribution of the bend in super-ellipse polar coordinates (θ_s, r_s). (d) Refractive index distribution of the bend in Cartesian coordinates.

Table 1. Parameters for Super-Ellipse Curves

	r_s(μm)	n_s
Inner boundary	$r_1 = 1.5$	$n_1 = 4.0$
Waveguide bend axis	$r_2 = 2.0$	$n_2 = 3.5$
Outer boundary	$r_3 = 2.5$	$n_3 = 3.0$

$$\kappa = \left| \frac{x'y'' - y'x''}{(x'^2 + y'^2)^{3/2}} \right|. \tag{2}$$

The curvatures of the inner boundary, axis, and outer boundary of the waveguide bend are shown in Fig. 1(b), indicated by solid, dashed, and dotted lines, respectively. As shown in the figure, for each super-ellipse curve, the curvature starts from zero at the input facet ($\theta_s = 0$), increases to its maximum at the middle of the bend ($\theta_s = 45°$), and then declines to zero at the output facet ($\theta_s = 90°$). Thus, if light propagates within the waveguide bend, the propagating light will be bent more strongly around the middle of the waveguide bend. Consequently, in the present design, we set the higher value of refractive index around the angle of $\theta_s = 45°$. Furthermore, as Fig. 1(b) also shows, the curvature along the inner boundary is larger than that along the axis as well as the outer boundary for any given angle of θ_s, which implies that the propagating light will be bent more strongly around the inner boundary relative to the axis or outer boundary. In view of this, in our design we set a higher refractive index around the inner boundary than we do along the axis or outer boundary. Based on the preceding curvature analysis, we set the refractive index profile of the waveguide bend as

$$n(\theta_s, r_s) = n_{\min} + (n_{\max} - n_{\min}) R(r_s) \Theta(\theta_s), \tag{3}$$

where the parameter $n_{\min} = 1.5$ is equal to the refractive index of the straight waveguide core, and $n_{\max} = 3.375$ is determined by optimization (see Section 3 for further details). $R(r_s)$ describes refractive index profile along the super-ellipse polar coordinates r_s, which is defined as

$$R(r_s) = \frac{r_3 - r_s}{r_3 - r_1}. \tag{4}$$

$R(r_s)$ is plotted in Fig. 2(a). Parameters r_1, r_3 are listed in Table 1. $\Theta(\theta_s)$ describes the refractive index profile along the super-ellipse polar coordinates θ_s, which is defined as

$$\Theta(\theta_s) = \begin{cases} \theta_s/\theta_a & \text{if } 0 \le \theta_s \le \theta_a, \\ 1 & \text{if } \theta_a \le \theta_s \le \frac{\pi}{2} - \theta_a, \\ \left(\frac{\pi}{2} - \theta_s\right)/\theta_a & \text{if } \frac{\pi}{2} - \theta_a \le \theta_s \le \frac{\pi}{2}. \end{cases} \tag{5}$$

$\Theta(\theta_s)$ is plotted in Fig. 2(b). The parameter θ_a in Eq. (5) is set to be 23.4°, which is determined by optimization (see Section 3). The refractive index profile along super-ellipse polar coordinates (θ_s, r_s) is plotted in Fig. 2(c) and is mapped into the Cartesian coordinates, as shown in Fig. 2(d), by using Eq. (1). In Fig. 2(c), the "flat top" width of $\Theta(\theta_s)$ seems to be larger than that of Fig. 2(d), which can be explained by the coordinate transformation. The "flat top" width of $\Theta(\theta_s)$ can be described by an angle of $\theta_{ws} = \frac{\pi}{2} - 2\theta_a = 43.2°$. In Fig. 2(d), the "flap top" width of $n(x, y)$ along polar coordinate θ can be calculated as $\theta_w = \frac{\pi}{2} - 2\arctan((\tan\theta_a)^{2/n_s}) \approx 23.3°$, which is roughly half of θ_{ws}. It is worthwhile to point out that the variable n_s in Eq. (1) is linear along the super-ellipse polar coordinate r_s,

$$n_s = n_1 - (n_1 - n_3)\frac{r_s - r_3}{r_1 - r_3}, \tag{6}$$

where n_1, n_3, r_1, and r_3 are listed in Table 1.

3. OPTIMIZATION AND PERFORMANCE OF THE WAVEGUIDE BEND FOR TE MODES

In this work, the waveguide bends are modeled and simulated using the finite element software package COMSOL. To optimize the waveguide bend for TE0 mode, TE0 mode fields are excited in the input straight waveguide at the wavelength of 1.55 μm. Then we use a very simple method to determine the parameters of $n_{\max}$ and θ_a in Eqs. (3) and (5), whereby we change their values alternatively and repeatedly until we obtain the optimal parameters of $n_{\max} = 3.375$ and $\theta_a = 23.4°$, with an optimal bending efficiency of $\eta_{\mathrm{TE0}} = 0.974$. The bending efficiency η_i is defined as the power transmission coefficient of

$$\eta_i = \frac{P^i_{\mathrm{out}}}{P^i_{\mathrm{in}}}, \tag{7}$$

where P^i_{in} and P^i_{out} are the input and output power of mode i. To estimate the coupling between the different modes, the crosstalk CT_{ij} are defined as

$$\mathrm{CT}_{ij} = 10\log_{10}\frac{P^j_{\mathrm{out}}}{P^i_{\mathrm{in}}}. \tag{8}$$

The power of different modes can be calculated using the overlap integral method [14]. For the optimized super-ellipse bend, the crosstalk between modes TE0 and TE1 is about −27 dB, corresponding to coupling coefficient below 0.002. The bending efficiency η_i and crosstalk CT_{ij} for the TE0 modes are also listed in the first column of Table 2. The distribution of the electric field component E_z is shown in Fig. 3(a), and Fig. 3(b) shows the field intensity $|E|$ along three transverse cross-sections, viz., the input facet $(y = 0, x > 0)$, middle of the bend $(y = x, x > 0)$, and output facet $(x = 0, y > 0)$, indicated by +,°, and ×, respectively. The symbol r represents $r = \sqrt{x^2 + y^2}$, where (x, y) are coordinates of the points along the transverse cross-sections. The dotted lines in Fig. 3(b) indicate the inner and outer boundaries of the waveguide bend at the input and output facets, for which $r = 1.5$ and 2.5 μm,

Table 2. Performance of the Designed Bend and Circular Bend for TE Modes, Including Bending Efficiency η_i and Crosstalk CT_{ij}

	Designed Bend		Circular Bend	
	TE0	TE1	TE0	TE1
η_i	0.974	0.742	0.494	0.266
CT_{ij} (dB)	−27.4	−27.8	−11.2	−11.3

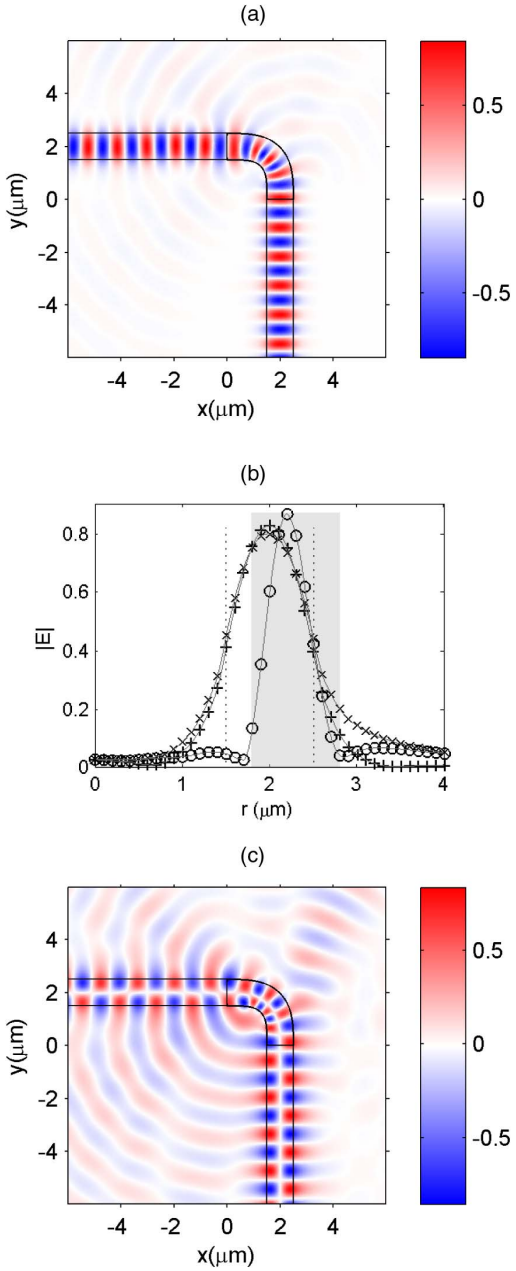

Fig. 3. (a) Field component E_z of the designed super-ellipse waveguide bend, TE0 mode. (b) Field intensity along three transverse cross-sections, viz., the input facet, middle of the bend, and output facet, indicated by +,°, and ×, respectively. The dotted lines indicate the inner and outer boundaries of the waveguide bend at the input and output facets, and the shaded area indicates the inner and outer boundaries at the middle of the bend. (c) Field component E_z of the designed super-ellipse waveguide bend, TE1 mode.

respectively. As shown in the figure, the full width at half-maximum (FWHM) width of the propagating field is about 1 μm at the input and output facets of the waveguide bend. The shaded area in Fig. 3(b) indicates the inner and outer boundaries at the middle of the bend (along the cross-section of $y = x$), for which $r = 1.78$ and 2.81 μm, respectively. Figure 3(b) shows that the FWHM width of the propagating field at the middle of the bend is approximately 0.5 μm, which is only half the width of that at the input and output facets. In addition, along the cross-section of $y = x$, the electric field intensity values at the inner and outer boundaries is 0.13 and 0.04 (arbitrary unit), respectively, which are much less than those at the input and output facets (between 0.39–0.45). Thus, the light propagating through the bend is confined within the core of the waveguide bend, which in turn helps to reduce the bending loss. Furthermore, from Figs. 3(a) and 3(b), we can infer that the incident light converges along the axis in the first half of the waveguide bend, then diverges in the second half of the bend, and finally transitions into the modal field of the output waveguide. The gradual transition of the propagating light may explain the efficient coupling between the waveguide bend and the straight waveguides. The designed waveguide bend with TE1 mode setting is also simulated, as shown in Fig. 3(c). From Fig. 3(c), we can see that the field radiates from the outer boundary, as well as from the output facet of the waveguide bend. The performance of the designed bend is also calculated numerically, as shown in the second column of Table 2. For TE1 mode, the bending efficiency η_{TE1} is 0.742, less than η_{TE0}, which can be explained by the comparatively smaller field confinement of the TE1 modes. We define the mode-confinement factor of the straight waveguide as

$$\Gamma = \frac{\int_{\text{core}} \mathbf{P} \cdot d\mathbf{s}}{\int_{\infty} \mathbf{P} \cdot d\mathbf{s}}, \tag{9}$$

where $\mathbf{P}$ is the time-averaged Poynting vector, and the integration is calculated along a transverse cross-section of the straight waveguide. By using Eq. (9), we find that $\Gamma_{TE0} = 0.925$ and $\Gamma_{TE1} = 0.599$. For TE1 mode, the mode field distribution expands more into the surrounding medium (air); thus, the propagating field is less affected by the bending core and experiences greater bending loss.

For the sake of comparison, a circular waveguide bend of similar size is also simulated. Figure 4 shows the simulation of a 90° circular waveguide bend, which has inner and outer boundaries of 1.5 and 2.5 μm in radius, respectively. The circular waveguide bend, as well as the input and output waveguides, have uniform refractive index of 1.5 in the core and the surrounding medium is air. The performance values of the circular bend are listed in the third and forth columns of Table 2. For the circular waveguide bend, the bending efficiencies are 0.494 and 0.266 for TE0 and TE1 modes,

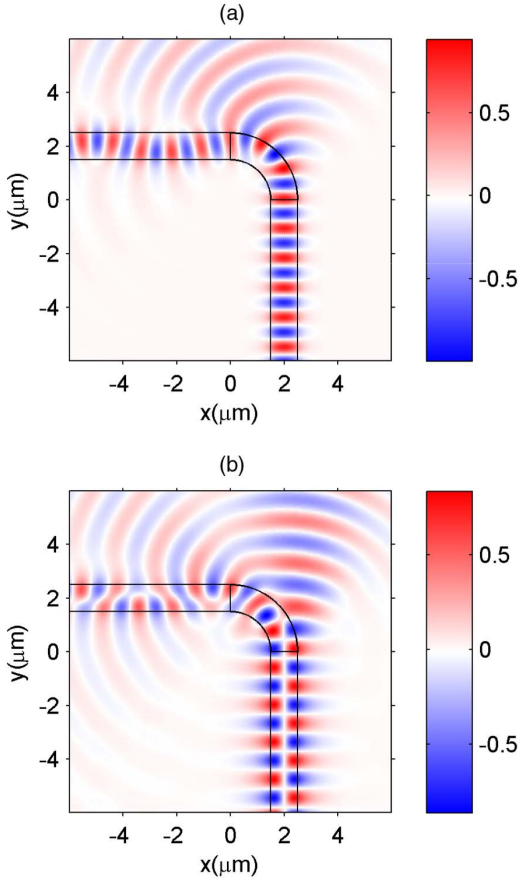

Fig. 4. Field component E_z of the circular waveguide bend for (a) TE0 mode and (b) TE1 mode.

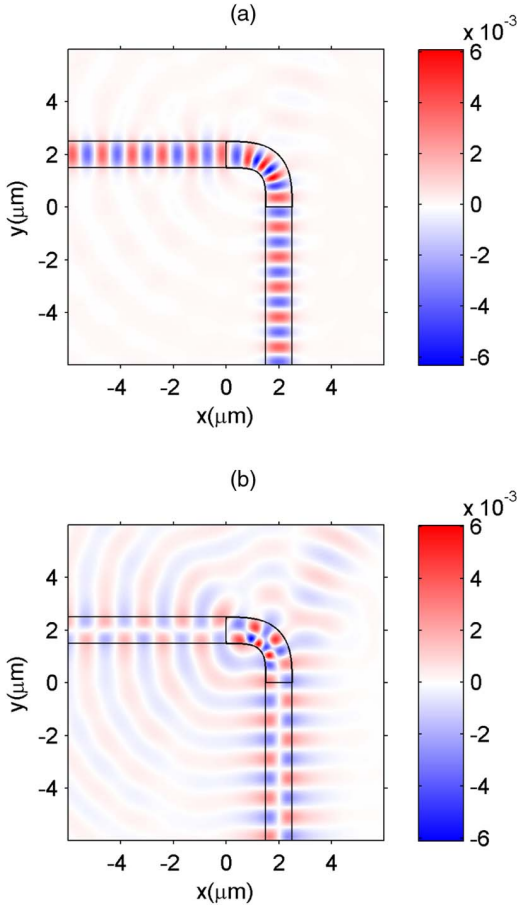

Fig. 5. Field component H_z of the designed super-ellipse waveguide bend for (a) TM0 mode and (b) TM1 mode.

respectively, which are significantly less than those of the proposed super-ellipse bend. We can clearly see the strong radiation around the circular waveguide bend in Figs. 4(a) and 4(b). In addition, Figs. 4(a) and 4(b) also clearly show the crosstalk of the TE0 and TE1 modes in the output straight waveguide. For the circular waveguide bend, the crosstalk between TE0 and TE1 modes is about −11.2 dB, corresponding to a power-coupling efficiency of about 0.0074 between the two modes.

4. PERFORMANCE OF THE WAVEGUIDE BENDS FOR TM MODES

The designed super-ellipse waveguide bend is also simulated with the TM0 and TM1 mode settings, as shown in Fig. 5. The performance of the designed waveguide bend is shown in the first two columns of Table 3. For TM0 and TM1 modes, the bending efficiency of the designed bend is $\eta_{TM0} = 0.958$ and $\eta_{TM1} = 0.478$, respectively. The TM0 and TM1 mode confinement factors of the straight waveguide are $\Gamma_{TM0} = 0.923$ and $\Gamma_{TM1} = 0.341$ respectively, which explains the higher bending efficiency for the TM0 mode and lower bending efficiency for the TM1 mode. The crosstalk between TM0 and TM1 modes is below −30 dB. The circular bend of the previous section is also simulated with the TM0 and TM1 mode settings, as shown in Fig. 6. It should be noted that in Fig. 6(b), the field distribution of H_z in the output straight waveguide is mainly TM0 mode and the incident field is only TM1 mode in the input waveguide. In case of exciting TM1 mode in the input waveguide, the output power carried by the TM0 and TM1 mode fields are $P_{out}^{(TM1)} = 0.026P_{in}^{(TM1)}$ and $P_{out}^{(TM0)} = 0.117P_{in}^{(TM1)}$, respectively; this is consistent with the field distribution H_z in Fig. 6(b).

Table 3. Performance of the Designed Bend and Circular Bend for TM Modes, Including Bending Efficiency η_i and Crosstalk CT_{ij}

	Designed Bend		Circular Bend	
	TM0	TM1	TM0	TM1
η_i	0.958	0.478	0.331	0.026
CT_{ij} (dB)	−33.8	−30.2	−9.28	−9.31

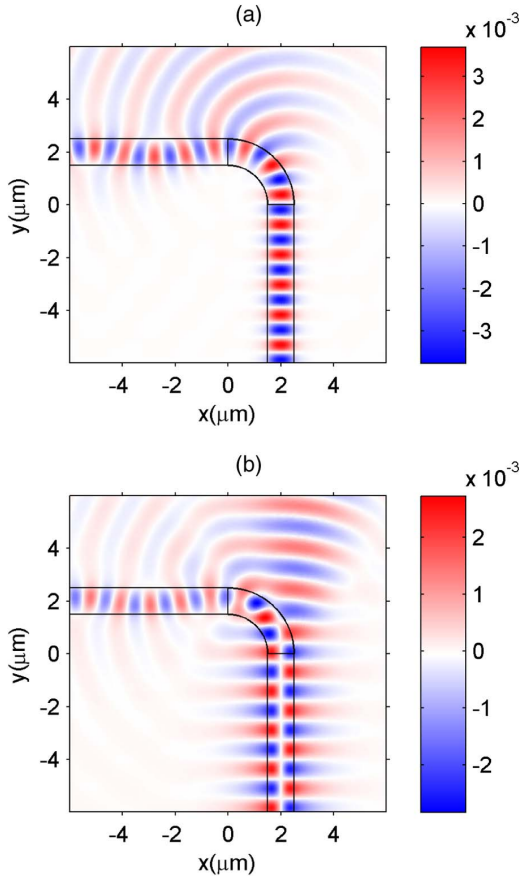

Fig. 6. Field component H_z of the circular waveguide bend for (a) TM0 mode and (b) TM1 mode.

5. DISCUSSION AND CONCLUSIONS

In this work, we have presented the design of a low-loss and compact optical waveguide bend which has super-ellipse boundaries and gradient refractive index structure in its core. First, the boundaries and axis of the waveguide bend are chosen to be super-ellipse curves. Next, the refractive index of the waveguide bend is set according to the curvature distribution of boundaries of the waveguide bend and its axis. Numerical simulations show that, for TE0 and TM0 modes of the input and output waveguides, light couples efficiently between the proposed waveguide bend and the input and output waveguides, and light that propagates through the bend is confined to the core of the waveguide bend. The design strategy used in this work is also useful for designing other compact optical and photonic components.

Considering the implementation of the proposed waveguide bend, one possible solution is to design and fabricate a sharp bend in a vertical slab waveguide [15] using the grayscale e-beam lithography, and control the height of the vertical slab waveguide to tailor the effective refractive index distribution in the bend core. Another possible solution is to design a sharp bend in a ridge waveguide consisting of graded photonic crystals (GPhC) [16], whereby the GRIN structure in the bend core can be implemented by spatially varying the sizes of the dielectric rods or air holes of the GPhC.

Funding. National Natural Science Foundation of China (NSFC) (51675506, 61377058); China Scholarship Council (CSC) (201506175051).

Acknowledgment. Y. Cao gratefully acknowledges the support of the CSC. Z. Liu and J. Zheng gratefully acknowledge the support of the NSFC.

REFERENCES

1. B. Rahman, D. Leung, S. Obayya, and K. Grattan, "Numerical analysis of bent waveguides: bending loss, transmission loss, mode coupling, and polarization coupling," Appl. Opt. **47**, 2961–2970 (2008).
2. P. Bienstman, E. Six, M. Roelens, M. Vanwolleghem, and R. Beats, "Calculation of bending losses in dielectric waveguides using

Eigenmode expansion and perfectly matched layers," IEEE Photon. Technol. Lett. **14**, 164–166 (2002).
3. W. Berglund and A. Gopinath, "WKB analysis of bend losses in optical waveguides," J. Lightwave Technol. **18**, 1161–1166 (2000).
4. A. Nesterov and U. Troppenz, "A plane-wave boundary method for analysis of bent optical waveguides," J. Lightwave Technol. **21**, 2434–2437 (2003).
5. Y. A. Vlasov and S. J. McNab, "Losses in single-mode silicon-on-insulator strip waveguides and bends," Opt. Express **12**, 1622–1631 (2004).
6. M. L. Calvo and V. Lakshminarayanan, eds., *Optical Waveguides: From Theory to Applied Technologies* (CRC Press, 2007).
7. M. Antelius, K. B. Gylfason, and H. Sohlström, "An apodized SOI waveguide-to-fiber surface grating coupler for single lithography silicon photonics," Opt. Express **19**, 3592–3598 (2011).
8. D. A. Roberts, M. Rahm, J. B. Pendry, and D. R. Smith, "Transformation-optical design of sharp waveguide bends and corners," Appl. Phys. Lett. **93**, 251111 (2008).
9. Z. L. Mei and T. J. Cui, "Arbitrary bending of electromagnetic waves using isotropic materials," J. Appl. Phys. **105**, 104913 (2009).
10. W. Ding, D. Tang, Y. Liu, L. Chen, and X. Sun, "Arbitrary waveguide bends using isotropic and homogeneous metamaterial," Appl. Phys. Lett. **96**, 041102 (2010).
11. B. Shen, R. Polson, and R. Menon, "Metamaterial-waveguide bends with effective bend radius $<\lambda_0/2$," Opt. Lett. **40**, 5750–5753 (2015).
12. D. Marcuse, *Theory of Dielectric Optical Waveguides* (Academic, 1974).
13. E. Kreyszig, *Differential Geometry* (Dover, 1991).
14. R. R. A. Syms and J. R. Cozens, *Optical Guided Waves and Devices*, 1st ed. (McGraw-Hill, 1974).
15. L. H. Gabrielli, D. Liu, S. G. Johnson, and M. Lipson, "On-chip transformation optics for multimode waveguide bends," Nat. Commun. **3**, 1217 (2012).
16. B. Vasić, G. Isić, R. Gajić, and K. Hingerl, "Controlling electromagnetic fields with graded photonic crystals in metamaterial regime," Opt. Express **18**, 20321–20333 (2010).